Magneto-Electro-Mechanical Modeling of Magnetic Actuation Systems

Ofer Ezra and Mor Mordechai Peretz

The Center for Power Management and Mixed Signal IC
Department of Electrical and Computer Engineering
Ben-Gurion University of the Negev, Beer-Sheva, Israel
oferez@post.bgu.ac.il, morp@ee.bgu.ac.il, http://www.ee.bgu.ac.il/~pel

***Abstract*— This study presents a new modeling methodology for magnetic actuation systems (MAS) that can be realized on a single simulation platform and is applicable in the majority of present-day simulation tools. The main benefit of the modeling approach is that it significantly reduces the complexity and burden in the design and control of multidisciplinary systems. The method describes the behavior of the system by the physical representation of the individual counterparts. The behavior of an actuator is described by cross-coupled models of the mechanical and the electromagnetic interaction. An extended, non-linear inductor model has been developed, demonstrating the challenging control task of displacement regulation. The MAS model and the individual models have been verified experimentally on a single-axis levitator prototype.**

***Keywords*— Magnetic actuation systems, modeling and simulation, non-linear inductor model, closed loop analysis, controller design**.

I. INTRODUCTION

Magnetic actuation systems (MAS) are used to levitate and stabilize floating or rotating systems without contact nor friction, replacing ordinary mechanical (passive) bearings. The non-contact property dramatically reduces the losses, and allows operation at higher mechanical speeds. This has increased the interest of such systems for a variety of applications, e.g., machine-tools (heavy-duty, high-speed, high-precision), flywheels for energy storage, turbo-molecular pumps, turbo-generators, aerospace positioning, and more [1]-[3]. An example of an emerging subject in the field of electromagnetic actuators is the active magnetic bearing (AMB). There, the aim is to eliminate the friction associated with the conventional ball bearings by using a set of strategically located, controlled, electromagnets to stabilize the location of the rotor in the free space (normally vacuum). By doing so, potentially lower power is required to maintain rotation and the speed can be increased since no heat is generated due to friction.

A simplistic electromagnetic actuation system (Fig.1) typically comprises an open-core inductive actuator that applies attraction force (Maxwell force) via its flux lines on a ferromagnetic element (e.g. iron). The actuator is fed by a current-controlled power driver such that the desired displacement (provided by an auxiliary control-loop) between the actuator and the element is maintained.

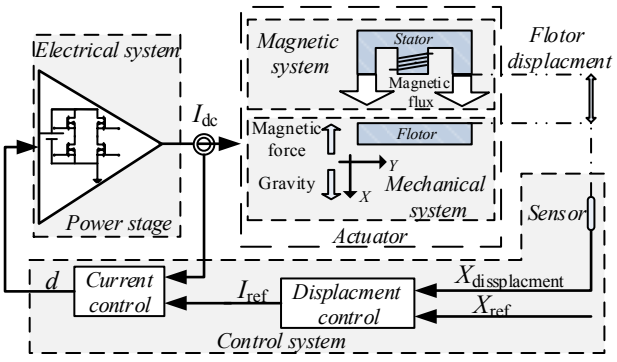

Fig. 1. Conceptual representation of a single-axis magnetic actuation system, divided into: electrical, magnetic, mechanical and control systems.

One of the main limiting factors that prevents MAS applications from being popular replacements to their mechanical precursors is the complex, and rather costly, control scheme and the associated circuitry that are required to facilitate high precision displacement control [3]. The reason for this obstacle is the lack of mutual interaction between mechanical, electromagnetics, and electrical engineers to provide an accurate definition and analysis tools for the multidisciplinary problem on-hand.

The concept of MAS, and AMB in particular, is widely covered in the mechanical engineering literature [4], including several potential solution for power drivers [2]. However, several assumptions and approximations that are commonly applied result in either poor closed-loop performance, or increased complexity of the end-product. For example, although the electromagnetic actuator is formed based on a variable-gap, variable-bias, magnetic element, its inductance in generally assumed as constant which prevents accurate design and prediction of the performance. Another example is that each of the units comprising the system (power stage, electromagnet, and controller) is analyzed and designed via a different platform with virtually no link of communication between the designs, which, in turn, adds complexity to the system.

The main objective of this study is to facilitate *a single platform, generic, modeling methodology for MAS applications* that is applicable in common simulation tools (e.g. Spice, PSIM, Matlab, etc.) and is based on the physical representation

of the system. In particular, this study provides a simple modeling extension for variable inductors as a function of both the bias current and the air-gap. The resulting *magneto-electro-mechanical model of the MAS* represents the complete system, including the controller, and therefore provides a straightforward platform for the development and design of such systems.

The modeling methodology is demonstrated in this study, without loss of generality, on a single-axis actuation system (generally for levitation) and combines three main building blocks. An actuator model (Section II) that comprises the mechanical and electromagnetic relationships, power stage modeling (Section III), and closed-loop design (Section IV). Model validation with experimental results are detailed in Section V.

II. ACTUATOR MODEL

A typical actuator (Fig. 2) is constructed of an open-core electromagnet that applies attraction force via its flux lines on a ferromagnetic element, named *flotor* [3]. The objective of the MAS system is to provide sufficient energy to the actuator such that the translated attraction force overcomes the other auxiliary forces and sustains the flotor within the desired displacement from the core. It should be taken into account, however, that the energy that is required to regulate the flotor may considerably vary as a function of the desired operating point, i.e. the air-gap. This is due to the fact that the magnetic energy ($LI^2/2$) depends on both the inductance and the drive current. To model this behavior, two cross-coupled behavioral blocks are applied, as can be observed in Fig. 2: One to model the mechanical impact [5]-[6], and the other to represent the inductance behavior.

The relationship between the sum of forces to the flotor displacement is by the mechanical system and can be expressed as

$$ma_{cc} = \sum F_{\text{external}} - F_{\text{magnetic}} \tag{1}$$

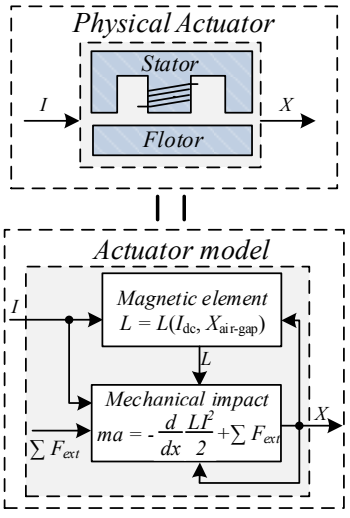

Fig. 2. Electromagnet model with two cross-coupled units: mechanical system and varible inductor.

where m and a_{cc} are the mass and acceleration of the flotor, respectively. $F_{\text{magnetic}} = -dw_x/dx$, the magnetic force is a results of the total energy of the actuator [3], hence the relationship

$$F_{\text{magnetic}} = -\frac{dw_x}{dx} = -\frac{d}{dx}\frac{LI^2}{2} \tag{2}$$

where $L(X_{\text{air-gap}}, I_{\text{dc}})$ is the inductance of the actuator at the operating point and is a function of the displacement $x_{air\text{-}gap}$, and the current through the actuator winding I_{dc}.

Without loss of generality, the force relationship for a single-axis actuator, as shown in Fig. 1, can be expressed using (1) and (2) as

$$a_{cc} = g - \frac{\frac{1}{2}\frac{d(LI^2)}{dx}}{m} \tag{3}$$

where $g \approx 9.8$ m/s^2 is gravity acceleration. Integrating the acceleration over time results in the velocity and displacement, x.

As can be observed in (2), the derivative of the magnetic energy with respect to the displacement is required to obtain the magnetic force. However, the majority of simulation tools apply time as the varying parameter. To overcome this obstacle, the following transformation is applied:

$$\frac{d}{dx}\left(\frac{LI^2}{2}\right) = \frac{d}{dt}\left(\frac{LI^2}{2}\right)\Big/\frac{dx}{dt} \tag{4}$$

which can be implemented using readily available embedded functions. Given the information on the constants, the inductance and the bias current, the model for calculating the force and flotor displacement is shown in Fig 3. To avoid potential convergence problems that are due to division by zero, a saturation element (e.g Etable in PSpice) may be applied to the calculation of dx/dt

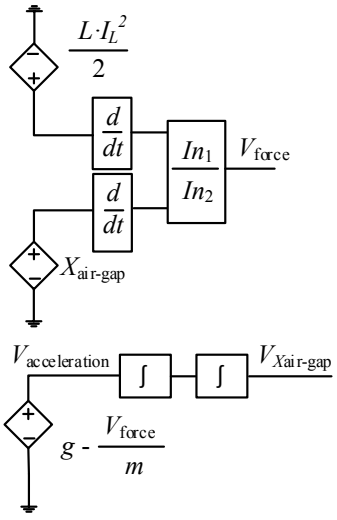

Fig. 3. Force and air-gap calculation.

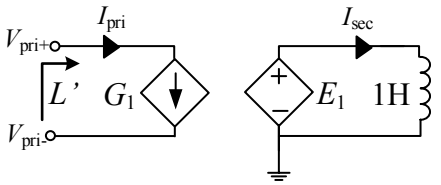

Fig. 4. Non-linear inductor model.

To express the inductance as a function of varying air-gap and bias current, an extension to the non-linear inductor model of [7] is applied. To model a non-linear inductance, the behavior of a linear inductor is reflected via a non-linear transformer, as shown in Fig. 4. The dependent sources are defined by

$$E_1 = \frac{V_{pri}^{+} - V_{pri}^{-}}{K}, G_1 = I_{sec}. \quad (5)$$

After some manipulations, the resulting inductance, reflected to the primary side can be expressed as

$$X_{L'} = \frac{V_{pri}^{+} - V_{pri}^{-}}{I_{pri}} = \frac{V_{sec} K}{I_{sec}} = X_L K. \quad (6)$$

If K is made dependent on the current through the inductor and on the air-gap, then the model emulates the non-linearity of the device. In the simulator environment, K can be defined as an expression.

To facilitate the dependence of the inductance on the displacement and the current, a reluctance model analysis approach is adopted [8]-[9]. In this method, the current through the winding is represented by a voltage source, flux is represented by current, and reluctance by resistance. Then, simple Kirchhoff's laws can be applied to extract the inductance as a function of the core geometric and magnetic characteristics. The model extraction is demonstrated here for an E-core type actuator, as shown in Fig. 5 as well as with the equivalent reluctance circuit.

The calculation for the resistances is as follows: for a component section of length l, cross-section A, and permeability μ, the resistance is

$$R = \frac{l}{\mu A}. \quad (7)$$

Following (7) and given the core dimension in Fig. 5 (a), the air-gap reluctance is $R_{gap} = l_g / (\mu_0 A_g)$ and the core section reluctance is $R_{core} = l_{core} / (\mu_0 \mu_r A_e)$, where A_g is the air-gap's cross section area, assumed equal to the core cross section area A_e. The specifications for the circuit reluctances are listed in Table I. The magneto-motive-force of the electromagnet as a function of the magnetic flux and core reluctances can be obtained using Ohm's law as

$$ni = \varnothing \sum R \quad (8)$$

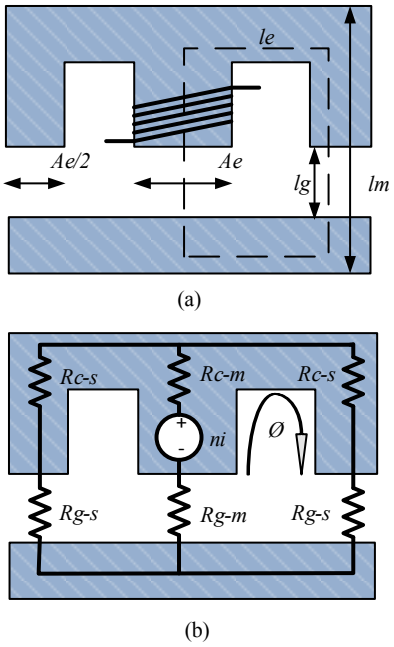

Fig. 5. An E-core actuator structure and dimensions, (b) the actuator reluctance model.

where n is the number of turns. Applying Faraday's law for induction, the voltage of the winding can be express as

$$V = n\frac{d\varnothing}{dt} = \frac{n^2}{\sum R}\frac{di}{dt} = L\frac{di}{dt}. \quad (9)$$

The inductance L can be extracted as

$$L = \frac{n^2}{\sum R(\mu_r, l_g)}. \quad (10)$$

TABLE I. RESISTANCES OF E-CORE RELUCTANCE MODEL

Section	Resistance
$R_{c\text{-}m}$	$\frac{l_e - l_m}{\mu_0 \mu_r A_e}$
$R_{c\text{-}s}$	$\frac{l_m}{\mu_0 \mu_r A_e / 2}$
$R_{g\text{-}m}$	$\frac{l_g}{\mu_0 A_e}$
$R_{g\text{-}s}$	$\frac{l_g}{\mu_0 A_e / 2}$

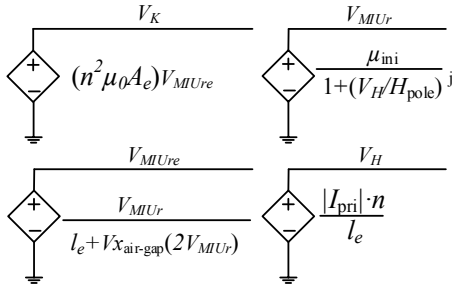

Fig. 6. Magnetic model for E-core actuator.

The equivalent total resistance, ΣR, is the additive sum of all the values form Table I is given by

$$\sum R = R_{g-m} + R_{c-m} + \frac{R_{g-s}}{2} + \frac{R_{c-s}}{2} = \frac{l_e + 2\mu_r l_g}{\mu_0 \mu_r A_e}. \quad (11)$$

Combining (10) and (11), the expression of L as a function of μ_r and l_g can be expressed as

$$L = \frac{n^2 \mu_0 A_e}{l_e} \frac{\mu_r(I_{dc})}{1 + 2\frac{l_g}{l_e}\mu_r(I_{dc})}, \quad (12)$$

l_g equals $X_{air\text{-}gap}$ and the permeability, μ_r, depends on the bias current and can be obtained from either the manufacturer data or by experiment [7]. A simplistic form of μ_r is given by

$$\mu_r = \frac{\mu_{ini}}{1 + \left(H / H_{pole}\right)^j}. \quad (13)$$

where μ_{ini} is the permeability initial value $\mu_{ini} = \mu_r$ ($H = 0$), H_{pole} is the magnitude of the saturation field and j sets the permeability slope. Variable H is proportional to bias current, $H = nI_{dc}/l_e$.

The actuator model obtained by (12) can be implemented in the simulation environment as shown in Fig. 6. Combining the models in Figs. 3, 4 and 6, yields the required cross-coupled model of the actuator. As can be observed, I_{dc} is assumed as an input to the model (from the power stage part) while other parameters are linked between the mechanical model (Fig. 3) and magnetic part (Fig. 6).

To validate the modeling approach, expression (12) derived based on theoretical analysis and manufacturer data has been compared with several experimental inductance curves as a function of the bias current, for several air-gap settings (15 µm, 100 µm, 130 µm). The actuator parameters were l_e = 68 mm, A_e = 69 mm^2, n = 17, H_{pole} = 30 A/m, j = 1.5757, μ_{ini} = 3000. The results are summarized in Fig. 7

III. Power Stage

A typical power driver configuration in MAS is realized by a full-bridge topology, operating in either complementary PWM, phase-shifted, or three-level switching scheme [11]-[13]. Full-bridge assembly is required to allow bi-directional current flow through the actuator which accelerates the construction of the attraction force. Since the object of the

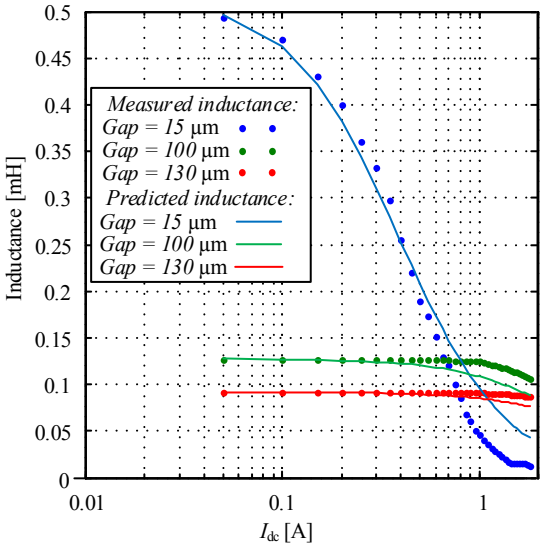

Fig. 7. Experimental results and the model simulation results

controller is the DC current through the actuator (which forms the attraction), a behavioral model approach [14] has been applied to model the average behavior of the driver. The average voltage across the actuator, assuming complementary PWM operation, can be expressed as

$$V_{L\_average} = V_{in}(2d - 1). \quad (14)$$

The power stage, a full-bridge topology and its behavioral model, which can be implemented in a numerical simulator is shown in Fig. 8.

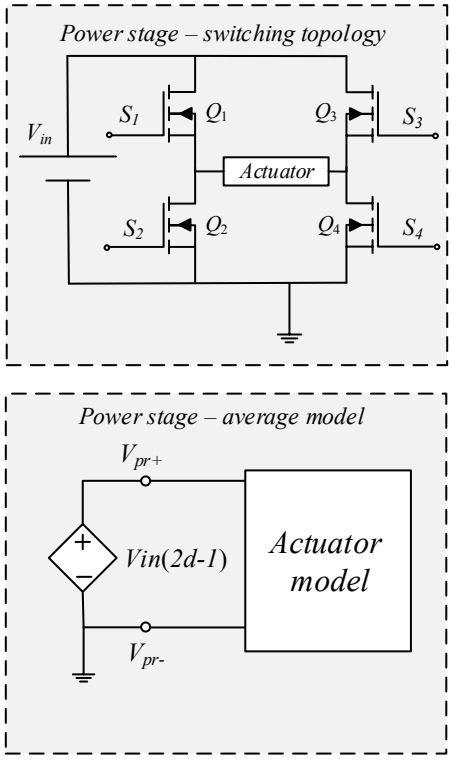

Fig. 8. Power stage and average model for complementary PWM

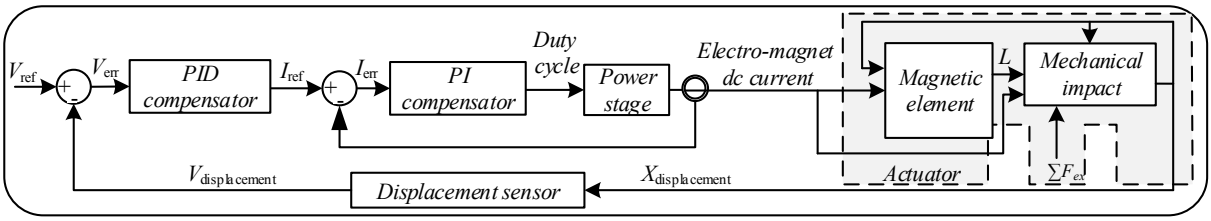

Fig. 9. Control system block diagram.

IV. Closed-Loop System

According the aforementioned analysis, the complete MAS model is constructed as shown in Fig. 9. As can be observed, the magnetic and mechanical variables are a function of the actuator bias current and the flotor displacement. To facilitate a simple controller structure, a two-loop approach is applied, an inner current control loop for the inductor current and an outer control loop for the flotor displacement. The compensation scheme design has been carried out on the basis that open-loop information of the system can be obtained by simulation; therefore, some of the manual derivation burden has been assigned to the simulator. In particular, once an initial current-loop controller has been assigned, the design of the outer loop controller has been carried out solely by simulation.

Based on the power stage model in (14), the inner current loop control-to-output transfer function (power stage plus inductance) can be expressed as

$$\frac{i_{L_{\text{average}}}}{d}(s) = \frac{2V_{\text{in}}}{sL(I_{\text{dc}}, X_{\text{air-gap}})}. \tag{15}$$

This implies that the dynamics of the system are strongly dependent on the operation point, as the inductance may significantly vary. Fig. 10 shows the control-to-output transfer functions of the inner current loop for several operating conditions (different air-gaps and bias current), as well as the selected compensation type (lag-lead). As can be observed, the compensator has been selected, in this simplistic design, to guaranty the system stability for the entire operation range.

The control-to-output frequency response of the outer displacement loop with the compensation scheme is shown in Fig. 11. It can be observed that the control-to-output transfer function $X_{\text{air-gap}}/I_{\text{dc}}(s)$ consists of 2 real poles, where one of them is located in the right half of the complex plane which implies instability of the system without proper compensation [3], [15]. In this study's extension, the actuators control-to-output transfer function can be expressed as:

$$\frac{x_{\text{air-gap}}}{i_{\text{actuator}}}(s) = \frac{k_i(X_{\text{air-gap}}, I_{\text{dc}})}{ms^2 - k_x(X_{\text{air-gap}}, I_{\text{dc}})}, \tag{16}$$

where k_i N/A is the force/current factor and k_s N/m is the force/displacement factor. As can be seen from (16), the poles of the system are with the same magnitude and differ only by sign, $\lambda_{1,2}=\pm(k_x/m)^{0.5}$. As a result, their influence on the open-loop phase is eliminated in specific frequency and manifests by providing 180 degrees phase lag throughout the frequency range, as can be seen in Fig. 11. Compensation for such system

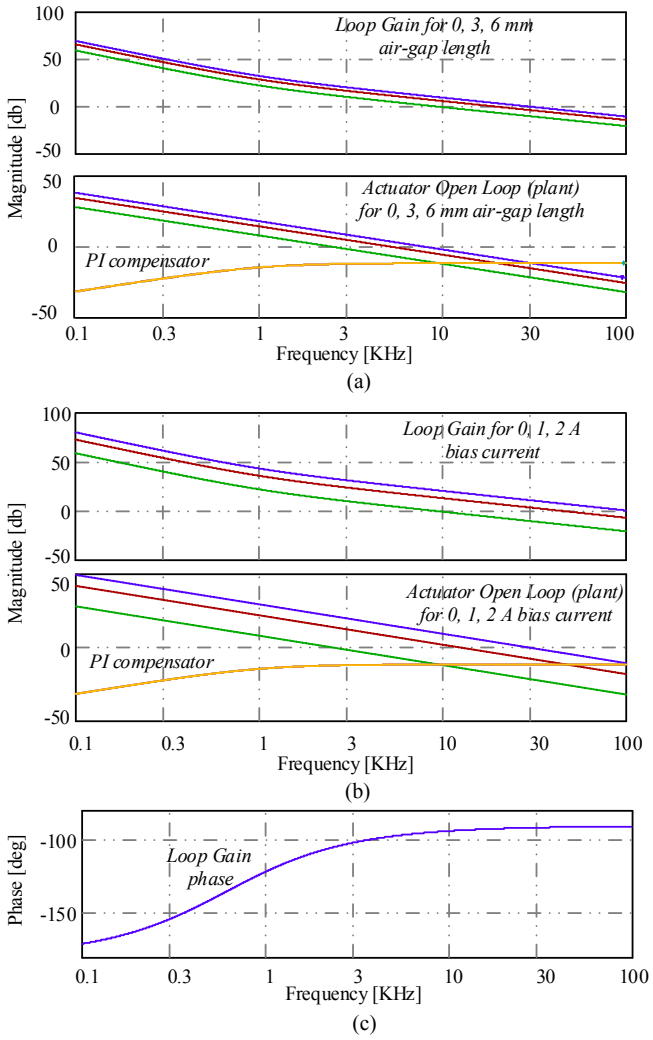

Fig. 10. Magnitude and phase of the inner loop for (a) different air-gap lengths with zero bias current (b) different bias currents with zero air-gap. (c) The loopgain phase, identical for all cases.

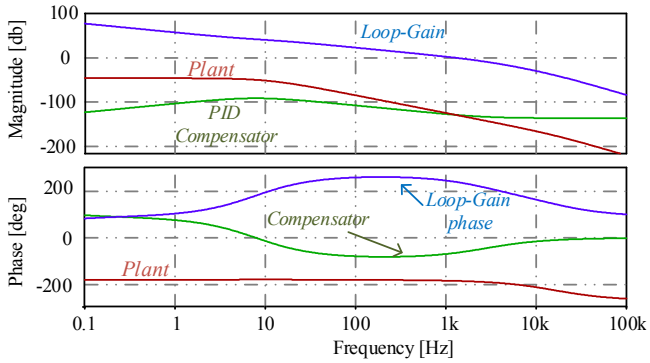

Fig. 11. Magnitude and phase of the outer loop

by linear control tools may be found challenging due to the non-minimum phase behavior of its roots. However, as can be seen in Fig, 11, for the particular frequency range of interest, i.e. beyond the double pole location, the behavior of the system resembles the classical minimum-phase, double pole configuration with 180 degrees phase lag, which can be effectively compensated by a double zero, i.e. PID, compensation scheme. This approach has been realized in the current study, as can be seen in Fig. 11. It should be noted, and can be observed that, the design of the outer loop is carried out under the assumption that the bandwidth of the inner loop is sufficiently larger that of the outer loop, therefore reducing the complexity of the compensator.

V. EXPIRIMENTAL CIRCUIT DESIGN

To validate the MAS model, an experimental setup comprising the power stage and actuator (Fig. 12. drive stage, input capacitors, etc. were omitted for simplicity), was developed and compared against the simulation results. The controller has been implemented digitally on a microcontroller platform (dsPIC33FJ16GS502). The actuator was constructed by half-E-core and for the flotor, an I-core element was used. The core magnetic parameters, as well as the power stage and the sensors parameters are presented in Table II. A switching frequency of 100 kHz was chosen for the full-bridge operation. Also included are DCR based current sensor [16] and a non-invasive displacement sensor [17].

A comparison against the simulation results were obtained for both the inner and outer loop operation. Figs. 13 and 14 show the step response to a change in the displacement reference and the system (and model) reaction in both the actual displacement signal and actuator current. As very good agreement can be observed, validating the model prediction capability and controller design.

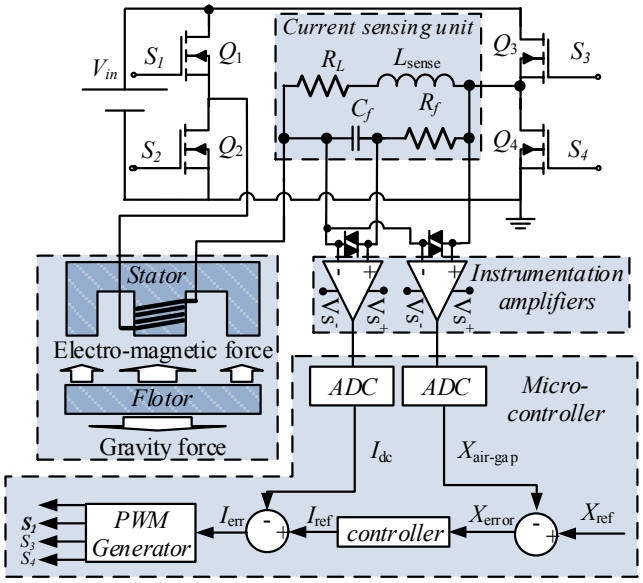

Fig. 12. Structure of actuator and current control system.

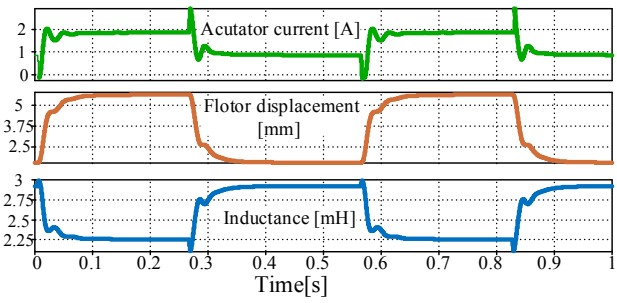

Fig. 13. Actuator current, displacement and inductance obtained by simulation.

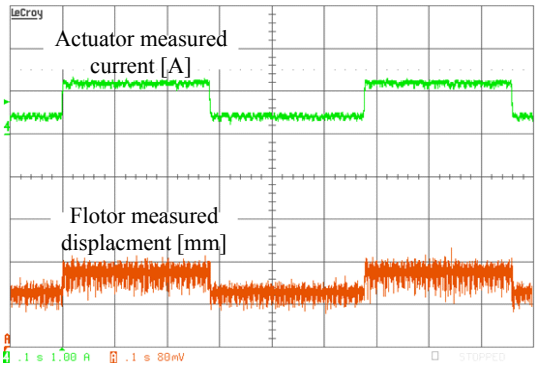

Fig. 14. Actuator current and displacement as measured by experiment.

TABLE II. EXPERIMENTAL AND SIMULATION COMPONENT SYMBOLS, VALUES AND MODELS

Actuator – Magneto-Mechanical stage		
Parameter	**Symbol**	**Value**
Core material		3F3
Effective length	l_e	130 mm
Effective area	A_e	540 mm^2
Flotor mass	m	35 g
Winding number	n	100
Power Stage		
Parameter	**Symbol**	**Value/Model**
Input voltage	V_{in}	20 V
Power transistors	$Q_{1\text{-}4}$	IPP030N10N3
Boot-strap drivers		IR2113
Gate resistors	R_{gate}	1 Ω
Pull down resistors	$R_{pull\text{-}down}$	10 kΩ
Displacement and current sensors		
Parameter	**Symbol**	**Value/Model**
Sensing inductor	L_{sense}	107 uH
Filter capacitor	C_f	5 uF
Filter resistor	R_f	200 Ω
Clamping diodes		1N5819
Instrumentation amplifiers		AD8428

VI. CONCLUSION

In this research, a novel modeling methodology for multidisciplinary applications such as MAS has been developed and verified by simulations and experiments. Cross influence of electrical, magnetic and mechanical parameters has been demonstrated through direct association between current, magnetic field, flux, magnetic energy, magnetic force, acceleration, velocity and distance. Thus, describing the actuator as a distance-related, current-dependent, variable inductor.

The operation of the MAS is demonstrated, without loss of generality, on a single-axis system with the flotor displacement as the main objective of the MAS controller. As shown throughout the derivations, by applying the required magnetic force (via the power driver), the controller accounts for the effect of the auxiliary forces such as gravity.

This study describes the behavior of an actuator as a variable inductor as a function of both the bias current and the air-gap, and can be applied to any magnetic core geometry. Using the resulting model, the control-to-output information of the system can be easily obtained for the entire operation range. As a result, the design of the compensations scheme can be carried out through the classical design tools. The overall model of the MAS is applicable in various numerical simulation tools, establishing a unified platform for the design of the electromagnets, controllers and power drivers.

REFERENCES

[1] B. Bolund, H. Bernhoff, M. Leijon, "Flywheel Energy and Power Storage Systems," *Elsevier*, vol. 11, pp. 235-258, 2007.

[2] A. Chiba, T. Fukao, O. Ichikawa, M. Oshima, M. Takemoto, D. Dorrell, *Magnetic Bearings and Bearingless Drives*, Newnes, Oxford, 2005

[3] G. Schweitzer, E. Maslen (eds.) *Magnetic bearings: theory, design, and application to rotating machinery*. Springer Verlag, Berlin, 2009.

[4] Y. Hung, N. G. Albritton, F. Xia, "Nonlinear control of a magnetic bearing system," *Mechatronics*, vol. 13, no. 6, pp. 621 – 637, 2003.

[5] J. D. Hewlett, B. M. Wilamowski, "SPICE as a Fast and Stable Tool for Simulating a Wide Range of Dynamic Systems," *International Journal of Engineering Education* 27(2), pp. 217-224, 2011.

[6] H. Toshiyoshi, "A Spice-based multi-physics simulation technique for integrated MEMS," *International Conference on Simulation of Semiconductor Processes and Devices* 2011.

[7] S. Ben-Yaakov, M. M. Peretz, "Simulation bits: a SPICE behavioral model of non-linear inductors," *IEEE Power Electronics Society Newsletter*, *Fourth Quarter*, pp. 9-10, 2003.

[8] R.W. Erickson, D. Maksimovic, "A multiple-winding magnetics model having directly measurable parameters," *IEEE PESC*, 1998.

[9] D. Medini, S. Ben-Yaakov, "A current-controlled variable-inductor for high frequency resonant power circuits," *IEEE Applied Power Electronics Conference and Exposition Conference Proceedings* 1994.

[10] J. D. Pollok, W. Lundquist, C. R. Sullivan, "Predicting inductance roll-off with DC excitations," *Proc. Energy Convers. Congress Expo*, pp. 2139–2145, Sep. 2011.

[11] Z. Changsheng, C. Yang, Z. Dan, C. Liang, "A current-control mode three-level PWM switching power amplifier for active magnetic bearings," *ICEMS, International Conference on*, pp. 2217-2220, 2008.

[12] Z. Changsheng and M. Zhiwei, "A PWM Based Switching Power Amplifier for Active Magnetic Bearings," *Proc. of 8th International Conference on Electrical Machines and Systems*, Nanjing. China, pp. 1563-1568, 2005.

[13] J. Wang, L. Xu, "Analysis and modeling of a switching power amplifier for magnetic bearing," *IEEE Industrial Electronics and Applications*, 4th IEEE Conference on, 2009.

[14] S. Ben-Yaakov, "Average simulation of PWM converters by direct implementation of behavioral Relationships," *IEEE Applied Power Electronics Conference*, pp. 510-516, 1993.

[15] G. F. Franklin, J. D. Powell, and M. L. Workman, *Digital Control of Dynamic Systems*, 3rd ed. Englewood Cliffs, NJ: Prentice-Hall, 1998.

[16] H. P. Forghani-zadeh, G. A. Rincon-Mora, "Current-sensing techniques for DC–DC converters," *in Proc. IEEE Midwest Symposium. Circuits and Systems*, vol. 2, pp. 577–580, Aug 2002.

[17] O. Ezra, M. M. Perez, "Study of magnetic actuation system," in *Electrical Electronics Engineers in Israel (IEEEI), IEEE 28th Convention*, Dec. 2014.